Metals and Materials International
https://doi.org/10.1007/s12540-020-00876-6

Numerical Analysis on Crack Generation Behavior of Hypo Peritectic Steel in Continuous Casting Process

Jun-hyun Jo[1] · Min-seok Park[2] · Kyung-woo Yi[1,3]

Received: 4 June 2020 / Accepted: 2 September 2020

Abstract
Hypo peritectic steels exhibit a high possibility of longitudinal crack during continuous casting. Therefore, many researchers have studied the mechanisms of crack generation in hypo peritectic steel. Stress in solidified shell, or volume contraction with small liquid fractions were suggested as the mechanisms of crack generation. A new model was developed for predicting possibility of crack generation by calculating strain rates in solid, volume contraction rate during solidification, and the probability of liquid unfilling in continuous cooling processes. The results show that massive transformation from the δ phase to the γ phase, and peritectic transformation during solidification can be the main crack generation mechanisms. Furthermore, a linear relationship exists between the amount of undercooling for peritectic transformation (dT_p) and the carbon content of the boundary for dividing the two crack generation mechanisms. Additionally, the longitudinal crack ratios of the field results are analyzed through strain rates in solid and liquid unfilling possibilities. Relative positions in the range of hypo peritectic steel and effective carbon contents are suggested to analyze the crack ratio of steels with alloying elements. This analysis shows that the results obtained from the new models for crack generation possibility are usable, and dT_p can generate the behavioral differences in crack generation according to the conditions.

Keywords Hypo peritectic steel · Modeling · Possibility of crack generation · Strain rate · Volume contraction

1 Introduction

Longitudinal crack generation on solidified slab surfaces is one of the major problems experienced in continuous casting processed. Especially, hypo-peritectic steels with approximately 0.09–0.16 wt% carbon are known to show high crack generation ratios [1, 2]. This phenomenon is generally believed to be influenced by peritectic transformation, as well as the solidification of the γ phase at the interface of the δ and L phases, at the early stage of continuous casting. Large volume changes by peritectic solidification and cooling may lead to the local deformation of the solidified shell, resulting in uneven heat transfer in the mold or stress generation on the shell surface, thereby causing cracks on the cast shell surface [2]. However, the exact mechanisms of surface cracks remain controversial.

Many researchers have suggested various crack generation mechanisms on the shell. Several groups have suggested that the stress generated inside the solidified shell during cooling and phase transformation is the main mechanism of crack generation in hypo peritectic steel [2–4]. Suzuki et al. proposed a stress index using the product of the volume change rate and the magnitude of volume change caused by cooling and phase transformation [2]. They opined that hypo peritectic steels have large stress index values due to phase change from the δ phase to the γ phase. Several computational models to calculate distribution of stress in the solidified shell have been developed for considering hypo peritectic steel behaviors [4–6].

Other groups have been interested in the remaining liquid fraction between dendritic arms during solidification, because their studies have shown that crack generations in the continuous casting process were evident in interdendrites [7]. These may be related to the inflow of the liquid phase into the dendritic arm spacing during solidification. Borland suggested that

✉ Kyung-woo Yi
yikw@snu.ac.kr

[1] Department of Materials Science and Engineering, Seoul National University, Seoul 08826, Republic Of Korea

[2] Technical Research Laboratories, POSCO, Kwangyang 57807, Republic Of Korea

[3] Research Institute of Advanced Materials, Seoul National University, Seoul 08826, Republic Of Korea

Published online: 16 October 2020

it was difficult for liquids to penetrate the dendrite arm spacing during solidification, especially when the liquid fraction was between 0.01 and 0.1 [8]. Consequently, Clyne et al. divided the mushy zone into the liquid feeding zone (0.4 < solid fraction (fs) < 0.9) and the cracking zone (0.9 < fs < 0.99) [9]. Since liquid can penetrate the dendrite arm spacing in the liquid feeding zone, the stress generated by phase change and cooling can be released by the refilled liquid. However, in the cracking zone, liquid cannot penetrate the dendrite arm spacing, because the channel narrows with lower liquid fractions. Xu et al. suggested a crack susceptibility index based on volume shrinkage during peritectic solidification and the remaining liquid phase [1]. They also suggested that liquid feeding into the dendrite arm spacing became difficult and the possibility of crack generation increased with solid fraction.

These two mechanisms are applicable to the solidification process of hypo-peritectic steels. However, previous studies related to the mechanisms had limitations that their algorithms assumed that all transformation processes occurred by diffusion-controlled transformation, and peritectic transformation started at the equilibrium temperature. However, various experimental results showed that the phase change behaviors of hypo-peritectic steels differed from those at the equilibrium state in continuous cooling. Lopez et al. analyzed temperature change during the solidification and phase transformation of hypo-peritectic steel, and they also calculated the first and second derivatives of the cooling curve [10]. Additionally, they reported that peritectic transformation started below the peritectic temperature and occurred within a temperature range. These phase transformation behaviors deviated from the equilibrium behaviors observed in other experimental results [11–13]. Furthermore, a massive transformation could occur during the solidification and phase transformation of hypo peritectic steel [14, 15]. Moon et al. reported that the speeds of the δ/γ interface were faster than 1 mm/s during the phase transformation from the δ phase to the γ phase, which could not be explained by diffusional transformation.

In the present study, volume contractions during solidification and cooling, ae well as strain rates and unfilling possibilities are calculated to estimate the crack susceptibility related to the crack formation model. Quantitative prediction for crack generation is calculated considering phase transformation and kinetics. The predictions of the possibility of crack generation are compared to the field results for model verification.

2 Modeling Procedure for Predicting Possibility of Crack Generation

Volume contraction by cooling and phase transformation can generate stress in shells. Thus, calculating the amounts and speeds of volume contraction are important to understand crack generation. To calculate volume contraction, it is assumed that phase transformation with peritectic transformation occurs mainly at the secondary arm spacing, according to Mondragon et al. [16]. This secondary arm spacing is affected by the carbon content and cooling rate. Moreover, solidification to the δ phase above the peritectic temperature occurs through dendritic growth during continuous casting. Therefore, a cylindrical domain with a diameter of the secondary arm spacing is used to evaluate volume change in this study. Eq. (1) is the secondary arm spacing suggested by Cicutti et al. [17] as follows:

$$\lambda_2 = 26.1 t_s^{0.38} \tag{1}$$

where λ_2 is the secondary arm spacing and t_s is cooling time of the primary δ phase.

Figure 1 represents the schematic diagram of phase change in hypo-peritectic steels by new models by considering the phase transformation behaviors deviated from the equilibrium behaviors [18]. In the two phase transformation paths of hypo-peritectic steels, the formation of the γ phase can be generated by diffusion-controlled transformation and massive transformation. In path 1, the liquid is solidified to the δ phase, which is then transformed to the γ phase by massive transformation. The γ phase is formed from the δ/γ interface with fast speeds of δ/γ interface calculated by the movements of iron atoms at a lattice parameter. In path 2, peritectic transformation starts at the δ/L interface during solidification to the δ phase, and solidification ends during the formation of the γ phase in the directions of liquid and δ phase. For phase transformation to the γ phase, carbon diffuses from the liquid, through the γ phase, to the δ phase. Furthermore, the total carbon amounts are constant during phase transformation. After solidification, the δ phase is transformed to the γ phase by diffusion-controlled transformation. At this stage, phase transformation to the γ phase is generated without carbon inflow from liquid. The formation speeds of the γ phase are calculated by carbon diffusion at the condition whereby the total carbon amounts are maintained. Consequently, the formation speeds of the γ phase differ from those of the phase transformation mechanisms. More details about this model have been explained in the literature [18].

These phase change behaviors in a cylindrical domain affect volume change, which by solidification and peritectic transformation, is generated at different speeds according to the phase change behaviors. Additionally, each phase contracts by cooling. Therefore, the effects of steel grades and temperature need to be considered for volume contraction during continuous cooling. In this study, density, which is affected by temperature and steel grades, is used for calculating the volume at each time step. Total density of the liquid, δ, and γ phases is obtainable by a simple mixture rule.

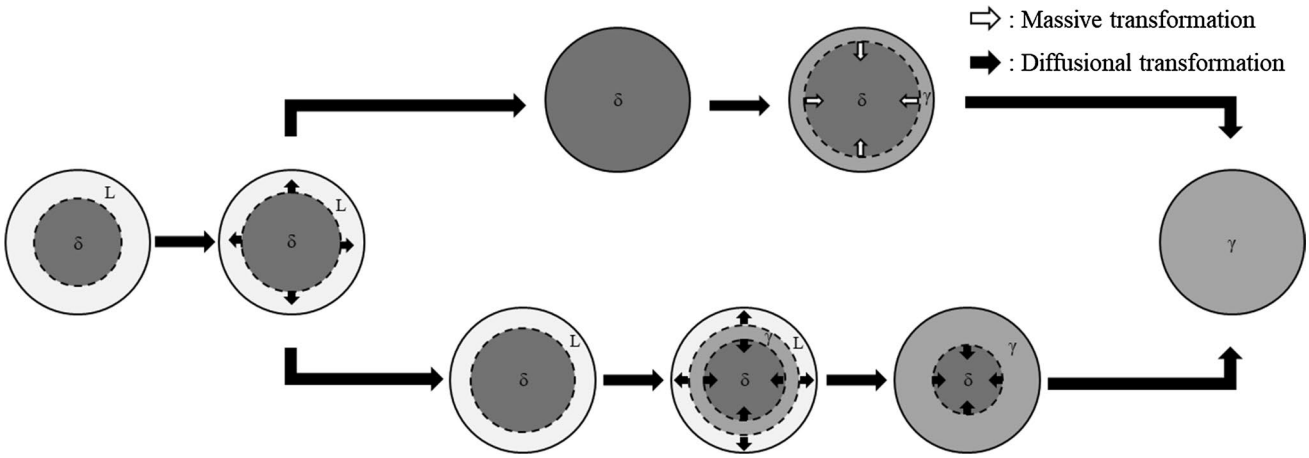

Fig. 1 Schematic diagram of phase change of hypo peritectic steel [18]

The following equations are used to determine the density according to the carbon content and temperature for each phase [19]. Afterward, the total volume per mass is calculated through the reciprocal of the total density.

$$\rho_{tot}\left(\frac{kg}{m^3}\right) = \rho_\delta f_\delta + \rho_\gamma f_\gamma + \rho_L f_L \tag{2}$$

$$\rho_\delta = \frac{100(8011 - 0.47T(°\mathrm{C})}{(100 - (wt\%C))(1 + 0.013(wt\%C))^3} \tag{3}$$

$$\rho_\gamma = \frac{100(8106 - 0.51T(°\mathrm{C})}{(100 - (wt\%C))(1 + 0.008(wt\%C))^3} \tag{4}$$

$$\rho_L = 7100 - 73(wt\%C) - (0.8 - 0.09(wt\%C))(T(°\mathrm{C}) - 1550) \tag{5}$$

$$V_{tot}\left(\frac{m^3}{kg}\right) = \frac{1}{\rho_{tot}} \tag{6}$$

As explained in the introduction, two crack generation mechanisms during continuous casting have been suggested in previous studies. In the first mechanism, the stress generated in the solidified shell during cooling is the main driving force. Stress is generated in the solid phase by cooling and phase transformation from the δ to the γ phase. Suzuki et al. suggested that the transformation rate and volume change of solidification, as well as the δ to the γ phase transformation, affected the stress in the solidified shell by using the relation between stress and strain, according to temperature [2]. Eq. (7) is a stress and strain relation according to temperature [20]. Where $\sigma, \epsilon, \dot{\epsilon}, Q, R, and\ T$ are the stress, strain, strain rates, activation energy, gas constant, and temperature, respectively.

$$\sigma = \mathrm{F} \times \varepsilon^n \times \dot{\varepsilon}^m \times \exp(-Q/RT) \tag{7}$$

Thus, it can be assumed that stress in the solidified shell is mainly determined by the strain rate.

The following equation is the strain rate in each time step that is used to predict the possibility of crack generation. The stress can be released when liquids exist together [9]. Therefore, strain rates are important after solidification is completed. Volume per mass can be used as the strain rate because the mass term is included in the numerator and denominator.

$$\dot{\varepsilon} = \frac{-(V_2 - V_1)/V_1}{dt} \tag{8}$$

$\dot{\varepsilon}$, V_1, V_2, and dt are strain rates, volume at the previous time, volume at the current time, and time step, respectively.

The second mechanism is related to liquid penetration into the dendrite arm spacing. Many researchers interested in this model suggested that thermal contraction and phase transformation could generate internal cracks during cooling, especially when the liquid fraction is smaller than 0.1 [7, 9, 21]. Therefore, it is assumed that the volume contraction rate is important for crack generation in the present model when solidification is incomplete. The penetration ability of liquids becomes poorer with larger volume contraction rates, and stress cannot be released when there is no liquid in the dendrite arm spacing; thus, cracks can be generated with large volume contraction with liquids.

For the volume contraction rate with liquid, the filling of liquids into the dendrite arm spacing must be considered, specifically when solidification is incomplete, because the volume is maintained by the filling of liquids. So, $V_{0,}$ the normalized initial volume of the calculated domain, is used as the denominator for the volume contraction rate, unlike

Eq. (8) of strain rate. Also, the amount of volume contraction can be considered as the amount of liquid that is filled at dendrite arm spacing newly. Thus, the following equation presents the volume contraction rate in each time step used to predict crack generation without liquids. $\dot{c_v}$, V_1, V_2, and dt represent the volume contraction rate, previous volume, current volume, and time step, respectively. These volumes are calculated using Eqs. (2–6).

$$\dot{c_v}(volume\ contraction\ rate\ with\ liquid) = \frac{(V_1 - V_2)/V_0}{dt} \quad (9)$$

The volume change (V_1–V_2) of Eq. (9) includes various behaviors of phase transformation and cooling. The volume change can occur by the cooling of each phase, solidification, and transformation from the δ phase to the γ phase.

Volume contraction rates are calculated for understanding the effects of volume change by cooling and phase transformation for crack generation, when the liquid fraction is small. However, the volume contraction rate with liquid is insufficient to comprehend the behaviors at the dendrite arm spacing for predicting the possibility of crack generation. Xu et al. suggested an index of solidification shrinkage by volume change during peritectic transformation and remaining liquid fraction after solidification. Moreover, it is revealed that this value is proportional to the crack ratio [1]. The following equation presents the index of solidification shrinkage (Rv) in this study.

$$Rv = \Delta V(1 - L) \quad (10)$$

where ΔV is the volume change by peritectic transformation and L is liquid fraction after peritectic transformation. Eq. (10) shows that the possibility of crack generation can increase with large volume shrinkage and small liquid fraction. Because the dendrite arm spacing, as the channel is filled by the liquid, becomes narrow, when liquid fraction is small. Therefore, it is difficult for the liquid to penetrate the narrow dendrite arm spacing and stress cannot be released.

In the present study, the liquid unfilling ability at the dendrite arm spacing is assumed to be an important factor to generate cracks. But, the effects of liquid unfilling for crack generation generation are considered differently from those of Xu et al. When the width of the liquid channel is narrow by a small liquid fraction, it can be assumed that the width of liquid channel is proportional to the liquid fraction while the pressure of the fluid at the channel is inversely proportional to the area of the channel. Therefore, it can be suggested that the penetration ability of the liquid into the dendrite arm spacing is inversely proportional to the liquid fraction. Consequently, it is propounded that the liquid unfilling possibility is inversely proportional to the liquid fraction. Thus, we define the liquid unfilling possibility as the maximum value of the volume contraction rate divided by liquid fraction, as shown in Eq. (11). The maximum values are used because crack generation probability is maximized at this condition.

$$\text{Liquid unfilling possibility} = \text{Maximum of}\left(\frac{Volume\ contraction\ rate\ with\ liquid}{Liquid\ fraction}\right) \quad (11)$$

3 Results and Discussion

3.1 Prediction Possibility of Crack Generation by a Model with Simple Peritectic Transformation Behaviors

3.1.1 Phase Fraction According to Temperature

The phase transformation of hypo-peritectic steels has been studied by many researchers [2, 22]. In their studies, the main phase transformation mechanism was carbon diffusion; it was assumed that the interfaces of δ/γ and γ/L were at local equilibrium, and peritectic transformation started at peritectic temperature. Furthermore, the massive transformation from the δ phase to the γ phase was not considered. Figure 2 depicts the change of phase fraction of Fe-0.095 wt% C and Fe-0.12 wt% C during cooling by using the assumptions of these studies. Liquid is solidified to the δ phase until peritectic temperature, whereby peritectic transformation starts. Once solidification completes, the δ phase is transformed to the γ phase. The difference between Fe-0.095 wt% C and Fe-0.12 wt% C is the amount of phase change by peritectic transformation. For Fe-0.095 wt% C and Fe-0.12 wt% C, the fractions of γ phase that remain are approximately 13% and 52%, respectively, after peritectic transformation. This is because more liquid remains at the peritectic temperature when the carbon content is 0.12 wt% C.

3.1.2 Volume Contraction Rates and Liquid Unfilling Possibilities During Cooling

Large volume contraction with small liquid fraction can cause liquid unfilling at the dendrite arm spacing, and subsequently, crack generation. To estimate the possibilities of this mechanism, volume contraction rates, according to carbon content, are calculated by using Eq. (9), as shown at Fig. 3a. The maximum volume contraction rates of Fe-0.095 wt% C and Fe-0.12 wt% C are generated when the liquid fractions are approximately 1.5% and 6.7%, respectively. These liquid fractions are the values when the temperature of each steel is peritectic temperature. At these conditions, maximum volume contraction rates are generated by

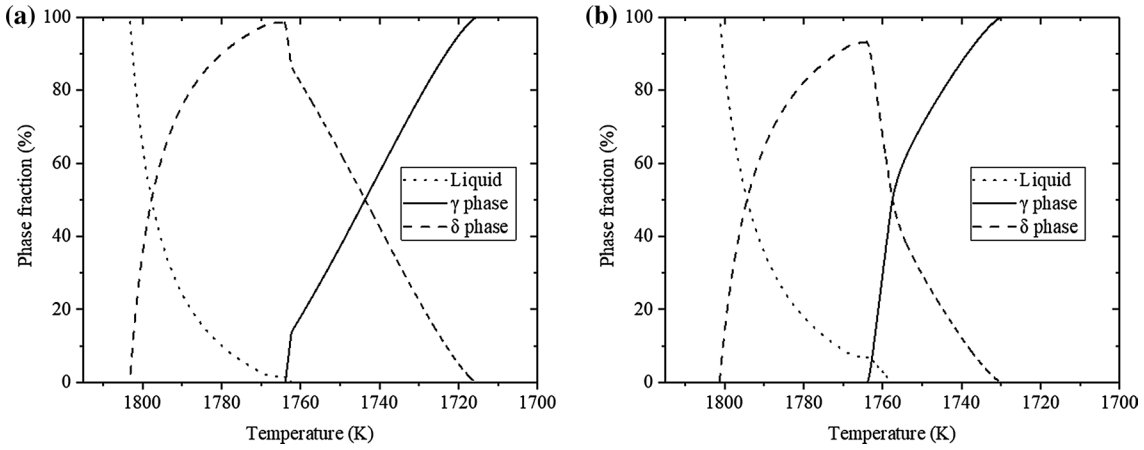

Fig. 2 Phase change according to temperature at 800 K/min by a model with simple peritectic transformation behaviors: **a** Fe-0.095 wt% C and **b** Fe-0.12 wt%

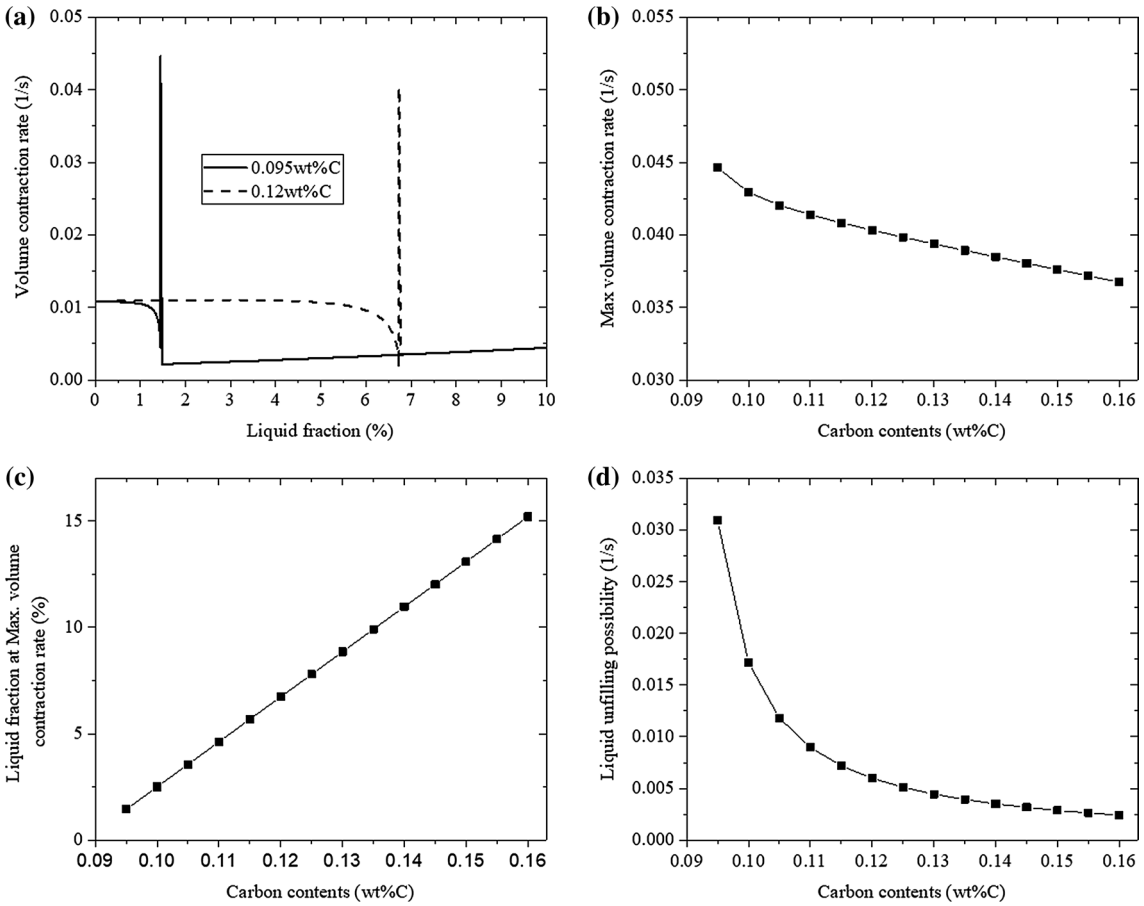

Fig. 3 Volume contraction rates, maximum volume contraction rates, and liquid unfilling possibilities by model with simple peritectic transformation behaviors

peritectic transformation ($L+\delta \rightarrow \gamma$). Because the volume of the γ phase is smaller than that of the liquid and δ phase, the total volume decreases by peritectic transformation. Thus, additional volume contraction by peritectic transformation is generated by comparing the cooling and solidification to the δ phase above the peritectic temperature. Additionally, the

volume contraction rates are generated by the fast peritectic reaction at the initial stage of peritectic transformation; subsequently, the volume contraction rates decrease rapidly and increase during solidification. At the peritectic transformation stage during solidification, the formation speeds of the γ phase are affected by the speeds of carbon diffusion. After peritectic transformation at peritectic temperature, the difference in the equilibrium carbon contents at the δ/γ and γ/L interfaces is small; thus, the speeds of phase transformation are lessened by the small carbon gradient in the γ phase. Moreover, the gradient of the carbon content in the γ phase increases, as do the speeds of peritectic transformation.

The maximum volume contraction rates according to carbon content are calculated as shown in Fig. 3b. These values are between 0.045 and 0.036 /s. Thus, the values of the maximum volume contraction rate are similar in the hypo-peritectic region. However, the liquid fraction values, whereat maximum volume contraction rates occur, are different when the carbon content change, as shown in Fig. 3c. Therefore, the liquid unfilling possibilities have a maximum value at 0.095 wt% C and decrease as the carbon content increases, as shown in Fig. 3d. These results suggested that cracks by liquid unfilling could easily occur at low carbon regions of hypo-peritectic steels.

3.1.3 Strain Rates in Solid Phase During Cooling

The strain rates in the solid phases of Fe-0.095 wt%C and Fe-0.12 wt%C are calculated from approximately 1762 K and 1757 K, respectively, and are shown in Fig. 4a. The peritectic transformations of Fe-0.095 wt%C and 0.12 wt%C start at the peritectic temperature, although the liquid fraction of the Fe-0.12 wt%C at the peritectic temperature is larger than that of Fe-0.095 wt%C. Therefore, the temperature at which solidification ends by peritectic transformation decreases as the carbon content increase. Both strain rates decrease from the maximum values because the width of the γ phase increases during its growth. As the width of the γ phase increases, so does the distance of carbon diffusion. Thus, the speeds of phase transformation decrease. The maximum strain rates, according to carbon content, are shown in Fig. 4b. The maximum strain rates decrease from 0.0059 to 0.0041 /s. Therefore, it can be suggested that the maximum strain rates are similar, according to the carbon content. Consequently, the effects of the carbon content on crack generation by this mechanism are minimal compared to maximum strain rates. Furthermore, it can be suggested that the maximum strain rates are very small. This suggestion is explained in the next section.

3.1.4 Analysis of the Crack Mechanism

Many researchers have suggested that large stress in the solidified shell and volume contraction with liquid unfilling can generate cracks during continuous casting. Therefore, crack generation behaviors can be analyzed with liquid unfilling possibilities, as presented in Fig. 3d and the maximum strain rates in Fig. 4b. The behaviors of crack ratio according to the carbon content tend to increase to the maximum crack ratio and decrease afterward [1, 23, 24]. Thus, the maximum crack ratio is generated at the mid-region of the hypo-peritectic steels. Notwithstanding, the liquid unfilling possibilities and strain rates of the solid calculated in the previous sections showed maximum values at the lowest carbon content, 0.095 wt%C, whereby phase transformation was assumed to start at the peritectic temperature. This implies that the experimental results cannot be explained by the previous calculations with simple peritectic transformation behaviors. Consequently, additional peritectic transformation phenomena need to be considered to explain the behavior of crack generation during continuous casting.

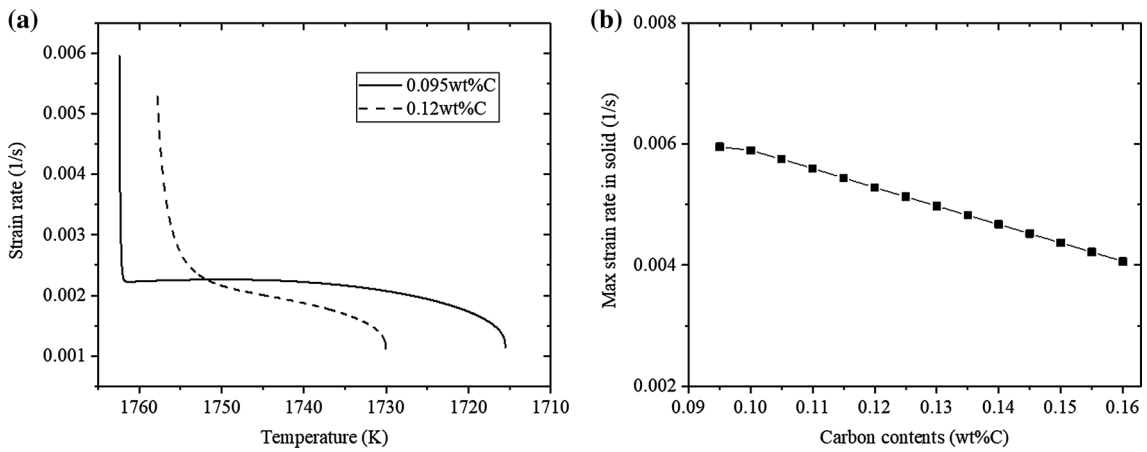

Fig. 4 Strain rates in solid phase and maximum strain rates by a model with simple peritectic transformation behaviors

3.2 Prediction Possibility of Crack Generation with New Phase Transformation Model

3.2.1 Phase Fraction According to Temperature

Previous models did not consider the behaviors of peritectic steels observed during experiments, such as the delay of peritectic transformation from the peritectic temperature [13, 15] and massive transformation [15, 25]. Recently, a model that considers these peritectic steel behaviors was developed [18]. In this model, the specific temperatures are defined; dT_p is the delayed temperature from the peritectic temperature until the formation of the γ phase, T_{ps} is a temperature at which peritectic transformation starts after the delay of the formation of the γ phase, and $T_{massive}$ is a temperature at which massive transformation starts. We calculate volume contractions and strain rates during cooling by adopting this phase transformation model. Figure 5 shows the change of phase fraction of each phase during cooling, when the cooling rate is 800 K/min and dT_p is 11 K.

The phase transformation behaviors of hypo-peritectic steels change according to carbon content, and dT_p that the delay of γ phase formation from the peritectic temperature. When the carbon content is 0.12 wt%C, the liquid is solidified to the δ phase until the peritectic temperature and additional solidification to the δ phase occur until T_{ps}, whereat the nucleation of the γ phase starts at the δ/L interface and the γ phase grows during cooling. Upon the completion of solidification, the δ phase that remains is transformed into the γ phase through diffusion-controlled transformation. When the carbon content is 0.095 wt%C, solidification to the δ phase starts from the liquidus temperature and concludes at a temperature between the peritectic temperature and T_{ps} without peritectic transformation. On cooling the solidified δ phase is until $T_{massive}$, the δ phase transforms to the γ phase by massive transformation. The speed of generation of the γ phase by massive transformation is faster than that that by diffusional transformation of Fe-012 wt%C.

3.2.2 Volume Contraction Rates and Liquid Unfilling Possibilities During Cooling

Figure 6 shows the volume contraction rates of Fe-0.095 wt%C and Fe-0.12 wt%C with liquid, when dT_p is 11 K. The volume contraction rates are the results when the liquid fraction is smaller than 10% because the movement of liquids into the dendrite arm spacing is difficult at this liquid fraction condition [8]. The volume contraction rates of Fe-0.12 wt%C have a peak at 2.2% of liquid fraction unlike that of Fe-0.095 wt%C. This is because peritectic transformation occurs during solidification, when the carbon content is 0.12

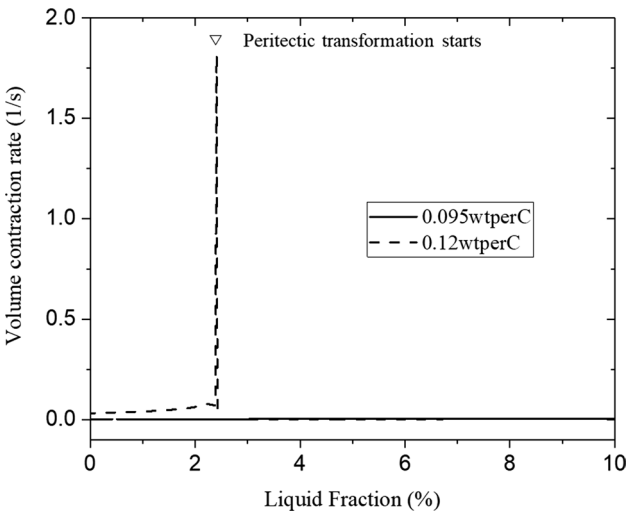

Fig. 6 Volume contraction rates with liquid when dT_p is 11 K

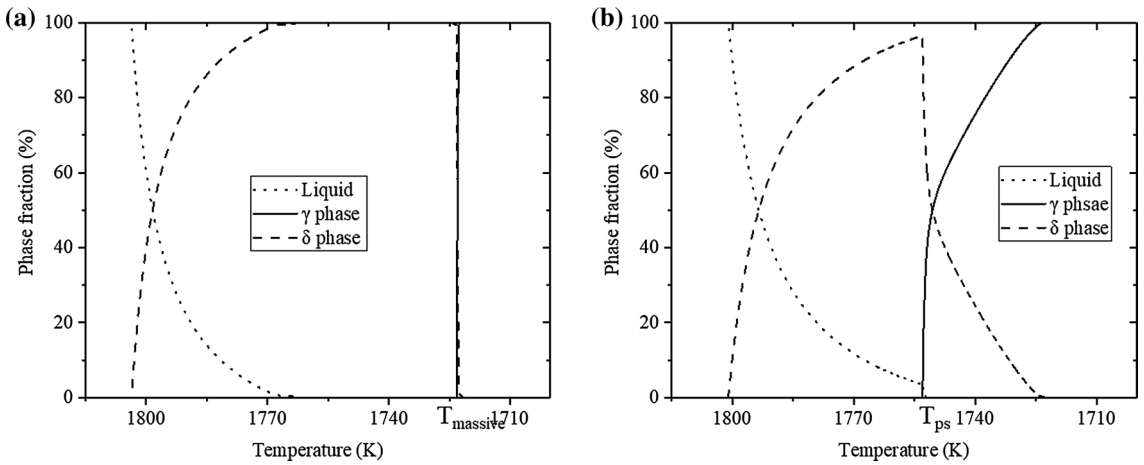

Fig. 5 Phase change according to temperature at a cooling rate of 800 K/min and 11 K of dT_p: **a** Fe-0.095 wt%C, **b** Fe-0.12 wt%C

wt%C. The volume change of Fe-0.095 wt%C is generated by cooling and solidification to the δ phase. However, the volume change of Fe-0.12 wt%C is generated by cooling, solidification, and peritectic transformation. In addition, transformation rates are very fast at the initial peritectic transformation stage [13, 18]. So, the volume contraction rates of Fe-0.12 wt%C exceed those of Fe-0.09 wt%C.

Maximum volume contraction rates with 11 K of dT_p are calculated according to the carbon content, as shown in Fig. 7b. The graph of maximum volume contraction rates can be separated into two parts: firstly, when the carbon content is less than 0.105 wt%C, the maximum volume contraction rates are approximately 0.02 /s, which is similar to the result of Fe-0.095 wt%C. Secondly, when the carbon content exceeds 0.11 wt%C, the maximum volume contraction rates are approximately 1.7 /s, similar to the results of Fe-0.12 wt%C. This difference is generated by the peritectic transformation according to the carbon content, as mentioned about volume contraction rates in Fig. 6. Consequently, it is revealed that phase transformation behaviors change by a specific carbon content, which is between 0.105 and 0.11 wt%C, when dT_p is 11 K.

In addition, when dT_p is 5 K and 20 K, the maximum volume contraction rates are calculated according to the carbon content, as shown in Fig. 7a and c. In these conditions, the maximum strain rates, according to the carbon content, can also be separated into two parts. However, the carbon content at which the maximum volume contraction rates increase rapidly is different. When dT_p is 5 K and 20 K, the maximum volume contraction rates increase rapidly at 0.10 wt% C and 0.125 wt% C, respectively. When the carbon content of steel increases, the liquid fraction increases at the peritectic temperature. And the more liquids can be solidified to the δ phase during dT_p, when dT_p is large. Because dT_p is the delay of the peritectic transformation from peritectic temperature. Thus, the solidification time to the δ phase increases with large dT_p. Consequently, when dTp increases, solidification can be completed at only the δ phase, without peritectic transformation during dT_p, irrespective of the increasing the carbon contents.

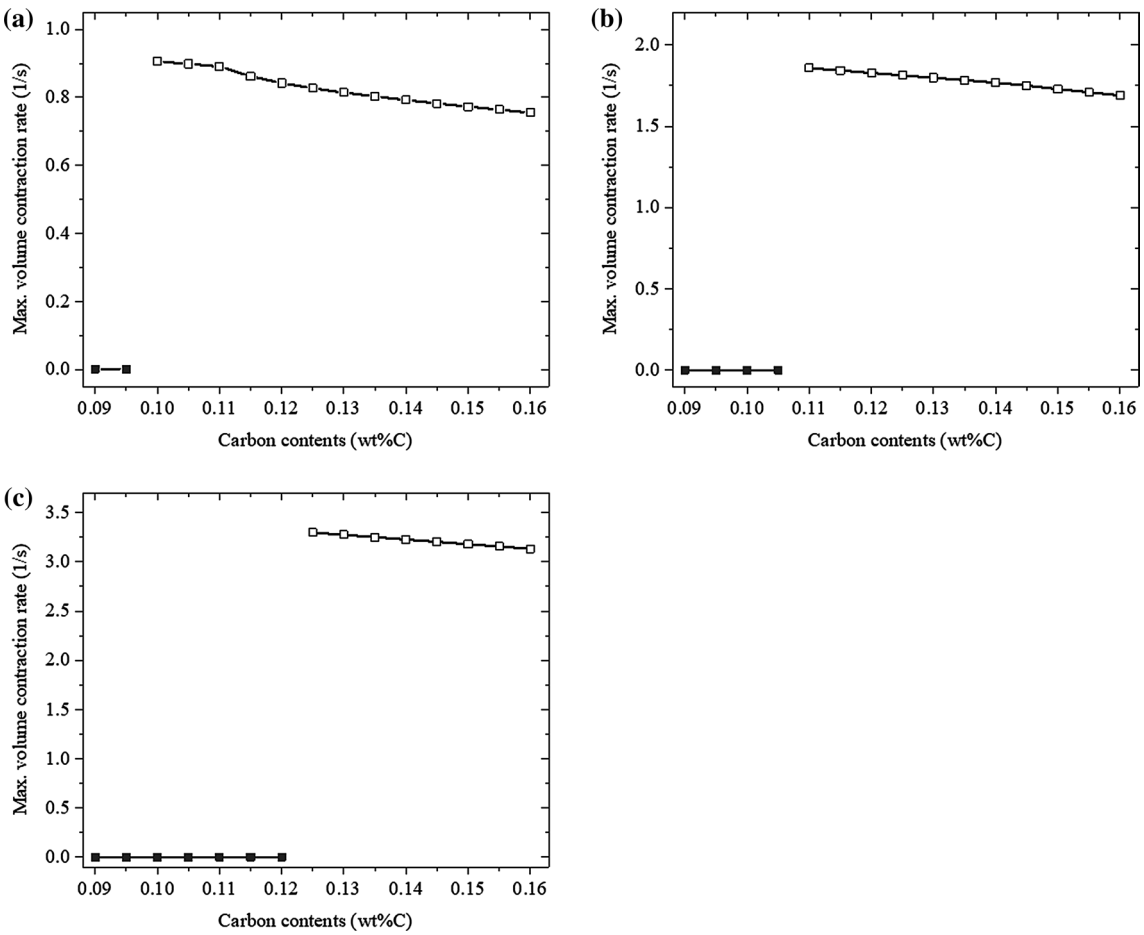

Fig. 7 Maximum volume contraction rates at 800 K/min with liquid: **a** $dT_p = 5$ K, **b** $dT_p = 11$ K and **c** $dT_p = 20$ K

Liquid unfilling possibilities at dT_p values of 5 K, 11 K, and 20 K are shown in Fig. 8. When dT_p is 11 K and the carbon content is less than 0.105 wt%C, the liquid unfilling possibilities are approximately 0.2 /s because there is no peritectic transformation during solidification. Liquid unfilling possibilities increase rapidly to 280 /s at 0.11 wt%C, similar to the maximum volume contraction rates, because large volume contraction occurs by peritectic transformation during solidification and the liquid fraction is very small at that time, while liquid unfilling possibilities decrease rapidly after 0.115 wt%C. This is because the liquid fraction at which maximum volume contraction rates are generated increases, although peritectic transformation occurs during solidification. Furthermore, when dT_p increases, the carbon content, at which liquid unfilling possibilities increase rapidly, increases by comparing the results of Fig. 8a–c. Because more liquid can be solidified to the δ phase without peritectic transformation during dT_p, when dT_p increases. This is also why the maximum volume contraction rates increase rapidly at specific carbon contents by increasing dT_p.

3.2.3 Strain Rates with Solid Phase During Cooling

Figure 9 displays the results of strain rates after solidification, when dT_p is 11 K. The strain rates of Fe-0.095 wt%C and Fe-0.12 wt%C start at approximately 0% and 27% of the γ fraction, respectively, because solidification is completed at these γ phase fractions. For Fe-0.12 wt%C, the strain rates decrease from 0.017 to 0.001 /s because the width of the γ phase at which carbon diffuses for phase transformation increases and there is no carbon inflow from the liquid due to the completion of solidification. For Fe-0.095 wt%C, the strain rates decrease from 0.06 to 0.001 /s. These values are larger than those of Fe-0.12 wt%C. Strain rates in solids show different behaviors depending on whether the phase change to the γ phase is diffusion-controlled or massive transformation, as shown in Fig. 5. When carbon content is 0.12 wt%C and dT_p is 11K, peritectic transformation starts during solidification. After solidification is completed by peritectic transformation, phase transformation from the δ phase to the γ phase occurs by diffusion-controlled transformation. However, when the carbon content is 0.095 wt%C

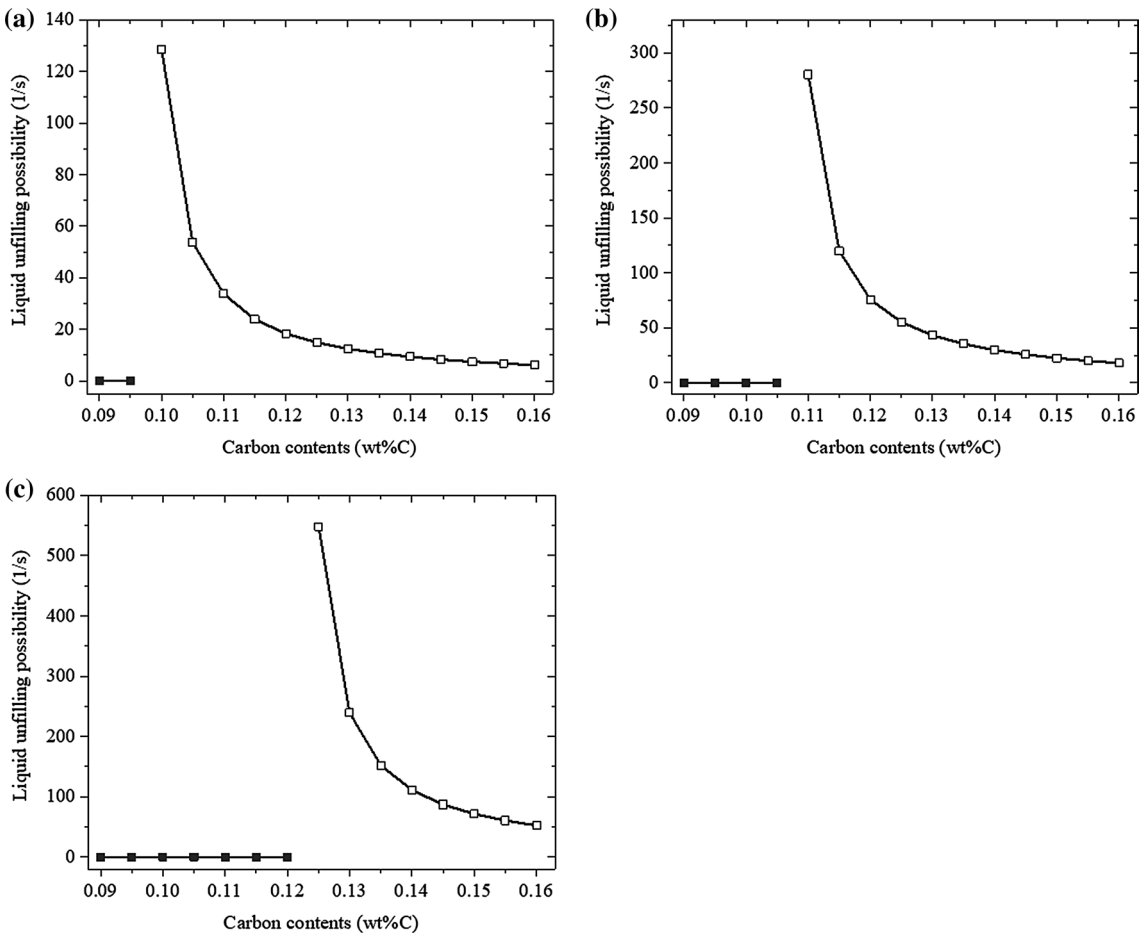

Fig. 8 Liquid unfilling possibilities at **a** $dT_p = 5$ K, **b** $dT_p = 11$ K and **c** $dT_p = 20$ K

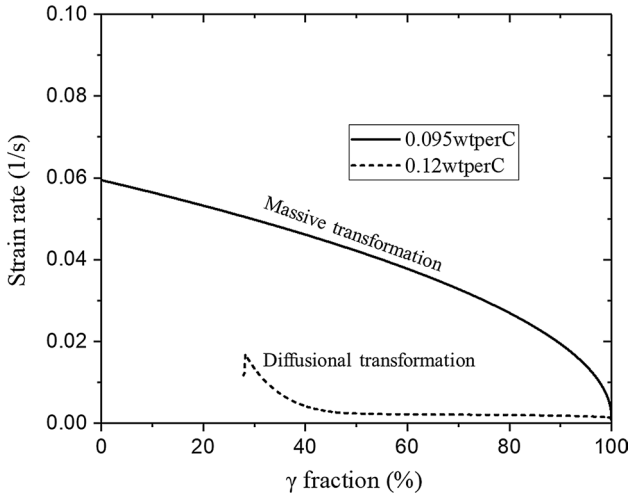

Fig. 9 Strain rates in solid without liquid when dT_p is 11 K

and dT_p is 11 K, solidification is concluded before T_{ps}, and it becomes the δ phase only, which is cooled until $T_{massive}$ and is converted to the γ phase by massive transformation. Thus, the mechanisms of phase transformation in solids are different, according to the carbon content. Moreover, the speeds of phase transformation by massive transformation are faster than those by diffusion-controlled transformation. Therefore, the strain rates of Fe-0.095 wt%C are faster than those of Fe-0.12 wt%C based on the difference of the transformation mechanisms in solids.

Large strain rates in solids can increase the possibility of crack generation. Therefore, the maximum strain rates with 11 K of dT_p are initially calculated according to the carbon content, as shown in Fig. 10b. When the carbon content is less than 0.105 wt%C, strain rates are approximately 0.23 /s, while at carbon contents larger than 0.11 wt%C, strain rates rapidly decrease to 0.035 /s, and the values further decrease to 0.01 /s. Maximum strain rates can be categorized into two parts according to the phase transformation behavior, such as volume contraction rates. When the carbon content is less than 0.105 wt%C, phase transformation from the δ

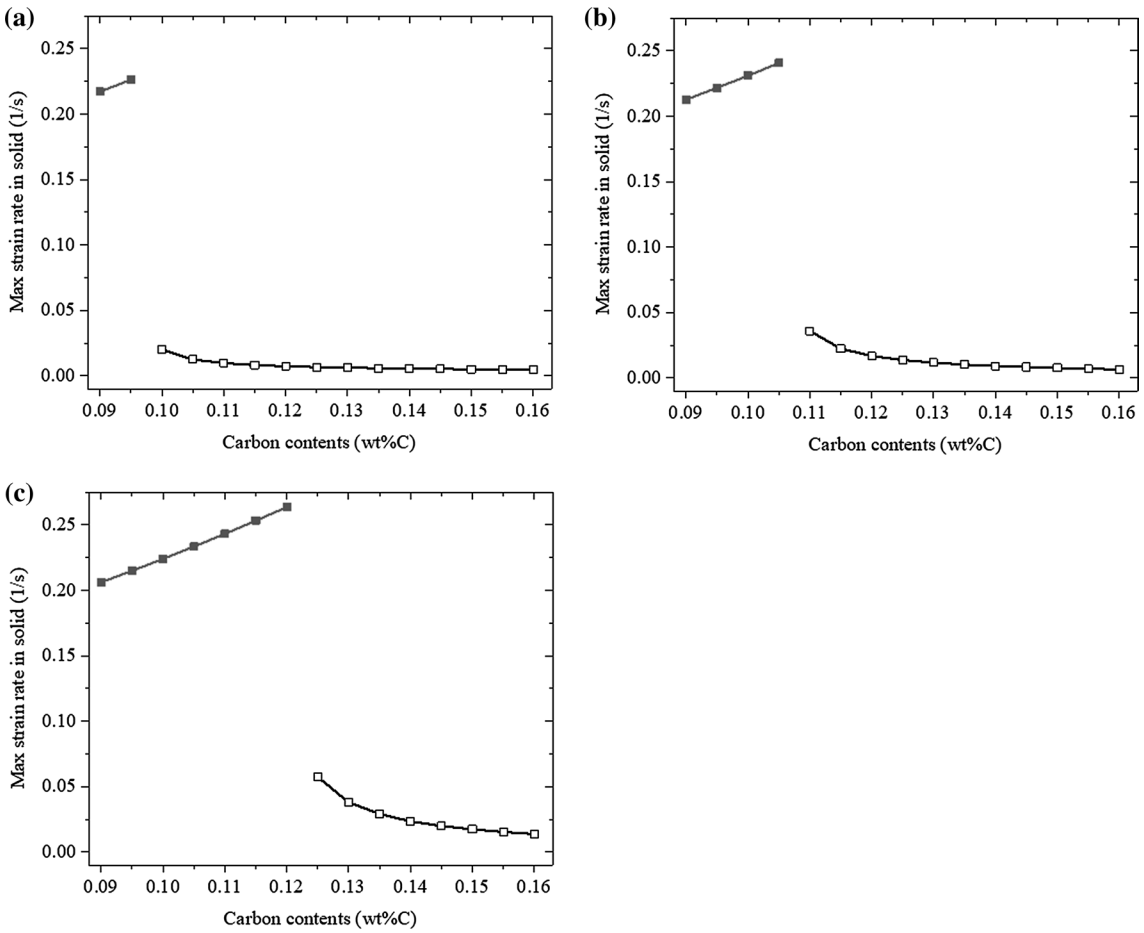

Fig. 10 Maximum strain rates in solid at 800 K/min **a** $dT_p = 5$ K, **b** $dT_p = 11$ K and **c** $dT_p = 20$ K

phase to the γ phase occurs by massive transformation. But, when the carbon content exceeds than 0.11 wt%C, phase transformation from the δ phase to the γ phase occurs by diffusion-controlled transformation. Thus, the mechanism of phase transformation from the δ phase to the γ phase determines the maximum strain rates in the solid phase. In addition, maximum strain rates with 5 K and 20 K of dT_p are calculated as shown in Fig. 10a and c. The carbon contents at which maximum strain rates decrease rapidly increase with increasing dT_p, because solidification can be completed to only the δ phase during dT_p, when dT_p is small. Therefore, phase transformation from the δ phase to the γ phase can be generated by massive transformation. Consequently, when dT_p increases, the strain rates in the solid are large at higher carbon contents, and cracks can be generated by massive transformation.

3.3 Mapping of Crack Generation Mechanism

From the results of the previous sections, it is revealed that the maximum strain rates and the liquid unfilling possibilities depend on the phase change behavior during and after solidification. These values are calculated to understand the mechanisms of crack generation during continuous casting. Higher volume contraction rates are generated by peritectic transformation during solidification, while higher strain rates are generated by massive transformation from the δ phase to the γ phase. Therefore, it is suggested that peritectic transformation during solidification and massive transformation in solids can be mechanisms of crack generation.

The results of Figs. 8b and 10b are compared to analyze the two crack mechanisms simultaneously. When the carbon contents exceed 0.11 wt%C, the liquid unfilling possibilities are large owing to peritectic transformation with liquid, and the maximum strain rates in the solid are small by diffusion-controlled transformation from the δ phase to the γ phase. Conversely, when the carbon content is less than 0.105 wt%C, the liquid unfilling possibilities are small because solidification only occurs to the δ phase without peritectic transformation, and the maximum strain rates in the solid are large by the massive transformation from the δ phase to the γ phase. In addition, the ranges of carbon contents at which maximum strain rates and liquid unfilling possibilities change rapidly, are the same. When dT_p is 11 K, this carbon content is approximately 0.107 wt%C. Furthermore, the largest values of the maximum strain rates in the solid and liquid unfilling possibilities are generated at approximately 0.107 wt%C. Thus, when dT_p is 11 K and the carbon content is approximately 0.107 wt%C, it can be suggested that the possibility of crack generation is largest. This shows that the behaviors of phase transformation and mechanisms of crack generation change based on these carbon contents. In addition, when dT_p values are 5 K and 20 K by comparing Fig. 8a, c, as well as Fig. 10a and c, the carbon contents whereby the strain rates and liquid unfilling possibilities change rapidly are approximately 0.096 wt%C and 0.121 wt%C, respectively. Consequently, these carbon contents increase, when dT_p increases. Figure 11 depicts the relationship between dT_p and carbon content based on crack generation mechanisms. To evaluate this relationship, the median values of the two carbon contents in the region where the crack generation mechanisms changed was used; when the dT_p changed by 0.1 K. In this study, the line representing the relationship between the carbon content and dT_p is defined as the transition line.

It is revealed that the main crack generation mechanisms are different on the left-hand and right-hand sides of the transition line by comparing Figs. 8 , 10, and 11. On the left-hand side of the transition line, the massive transformation with high transformation rates causes large strain rates after solidification. However, the solidification is completed without peritectic transformation, so liquid unfilling possibilities are low. On the right-hand side of the transition line, the liquid unfilling possibilities are high because of peritectic transformation during solidification. Nonetheless, maximum strain rates in the solid phase are low, because the phase change to the γ phase occurs by diffusion-controlled transformation. In other words, if dT_p is determined under specific process conditions by cooling rate or alloy elements, the main mechanism of crack generation can be selected according to the carbon content between the stress generated in the solid by massive transformation and liquid unfilling by peritectic transformation during solidification. Additionally, it can be suggested that the possibility of crack generation is high near the transition line, because the values of liquid

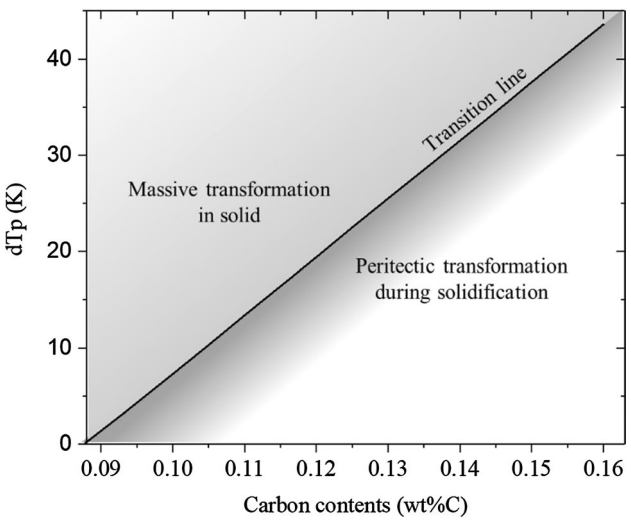

Fig. 11 Relationship between carbon contents and dT_p for phase change behaviors and mechanisms of crack generation

unfilling possibilities and maximum strain rates are highest near the transition line.

Alloy elements can change the behaviors of phase transformation. For example, Mn decreases peritectic temperature, while it increases the carbon content of peritectic points. Therefore, if Mn is added, many values used in the phase transformation model [18], such as equilibrium carbon content at each interphase and peritectic temperature, change. Thus, it is necessary to revise the phase transformation model for Fe–C–3.5Mn and 7Mn; the equilibrium carbon content at each interphase, as well as the specific temperatures, such as T_{ps}, T_{γ}, and $T_{massive}$, need to be modified in the phase change model. The local equilibrium carbon contents at the interphase and the peritectic temperature are calculated by FactSage to revise the model.

However, carbon diffusion is the main mechanism of phase transformation, such as for the Fe–C binary system, under these conditions, because the diffusivity of C is far larger than that of alloying elements, such as Mn and Si. At 1700 K, the diffusivities of C, Si, and Mn at the δ phase are $4.01 \times 10^{-5} cm^2/s$,$1.79 \times 10^{-7} cm^2/s$, and $9.65 \times 10^{-8} cm^2/s$, respectively [26]. The movement of carbon can drive peritectic transformation, even in alloy steels; thus, it can be assumed that the processes of phase transformation are the same as those of the Fe–C binary system.

As a result of the phase transformation model revised for steels with Mn, Fig. 12 presents the transition line of Fe–C, Fe–C–3.5Mn, and Fe–C–7Mn according to the relative position in the peritectic steel region, which is used to compare the results of steels with different Mn contents. Therefore, these transition lines are similar, although the Mn contents are different, which shows that steels with different Mn contents have similar phase transformation and crack generation behaviors according to the relative position in the range of peritectic steel and dT_p. The behavior of alloy steels can be explained by using the results of the Fe–C binary system, when the effective carbon contents are used.

3.4 Comparison Between Model Results and Field Data of Crack Ratio

Figure 13 presents the normalized longitudinal crack ratio data of approximately 40,000 continuous casting heats of a steel company, at -various alloying elements. These values were normalized based on the maximum longitudinal crack ratio. The composition ranges of the alloying elements used were 0–0.5 wt% for Si, 0–1.5 wt% for Mn, 0–0.05 wt% for P, 0–0.015 wt% for S, and 0–0.06 wt% for Al for analyzing the behaviors of crack generation. Consequently, it is revealed that the crack ratios of carbon contents between 0.05–0.1wt%C are irregularly scattered in the carbon contents. However, these results include the effects of various alloying elements, such as S and Mn. From the results shown in Fig. 12, the phase transformation behaviors of alloy steels can be analyzed by using their relative position in the range of peritectic steels. Therefore, in this study, the relative position in the range of hypo-peritectic steel (R) is proposed to apply crack data with various alloying elements to the results of phase change model. The relative position in the range of hypo-peritectic steel is newly modeled such that it can be well-applied in the composition ranges of the alloying elements to be analyzed.

The method to calculate the relative position in the range of hypo-peritectic steel is as follows: firstly, peritectic starting points and peritectic points of steels with various alloy

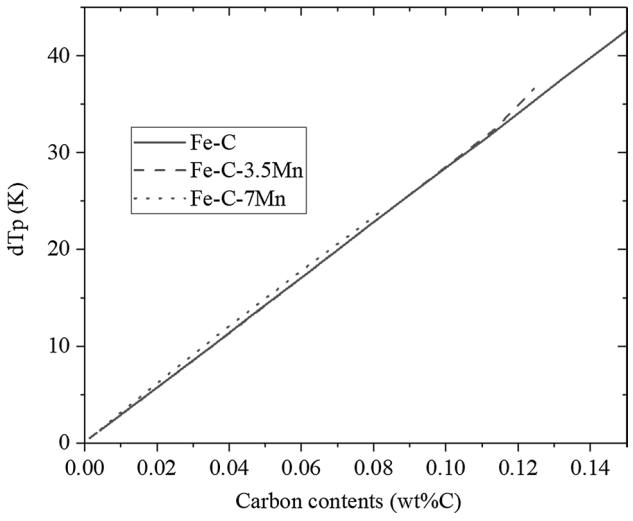

Fig. 12 Relationship between relative position in the region of peritectic steel and dT_p for crack generation mechanism according to Mn contents

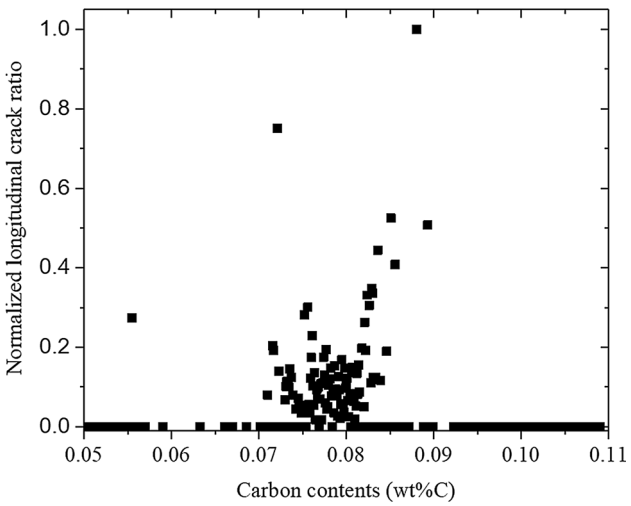

Fig. 13 Normalized longitudinal crack ratio according to carbon concentration

element compositions are calculated by using FactSage. Secondly, peritectic starting points(a) and peritectic points(b) are substituted into the equation of the relative position in the range of hypo-peritectic steel, as shown in Eq. (12).

$$R = \frac{x-a}{b-a} = \frac{1}{b-a}x + \frac{-a}{b-a} = Ax + B \tag{12}$$

x represents the carbon content of steel used to calculate the relative position in the range of hypo- peritectic steel.

In Eq. (12), A and B are composed of peritectic points (a and b), so they can be also considered as values depending on the alloying element composition. Thus, It is necessary to understand the effects of alloying elements on A and B to analyze the results of steels with various alloy element ratios. Firstly, the equation considering the effects of alloying elements on A and B is as follows: (The values in parentheses are the concentration (wt%) of each alloying element)

$$A(\text{or B}) = \text{a(Al)} + \text{b(S)} + \text{c(P)} + \text{d(Si)} + \text{e(Mn)} + \text{f(S)(Mn)} + \text{g(Si)(Mn)} + \text{h} \tag{13}$$

The coefficients of the Eq. (13) were fitted using the peritectic points of 87 alloy steels calculated by means of FactSage. The composition ranges of the alloying elements used were 0–0.5 wt% for Si, 0–1.5 wt% for Mn, 0–0.05 wt% for P, 0–0.015 wt% for S, and 0–0.06 wt% for Al. The coefficients of the equations obtained by fitting are shown in Table 1. As a result of fitting the values, the R square values of A and B are 0.96 and 0.91, respectively. In addition, the peritectic starting points and peritectic points are calculated with the composition of 20 randomly selected alloy steels. It is shown that the differences between the results by fitting equation and the values calculated by thermodynamic calculation by FactSage are within 0.001 wt%C. Thus, it is evident that the relative position in the range of hypo-peritectic steel can be used to compare the crack ratio data of different alloying steels.

In addition, the effective carbon contents (C_{eff}) can be calculated by the peritectic points of carbon steel and the relative position in hypo-peritectic steel (R) by using Eq. (14).

$$C_{eff} = 0.09 + R(0.16 - 0.09) \tag{14}$$

By using Eq. (12), (13), and (14), the longitudinal crack ratio data in Fig. 13 can be transformed based on the effective carbon contents. Figure 15 presents the values of the longitudinal crack ratios every at intervals of 0.04 of effective carbon contents. These values are normalized based on the maximum longitudinal crack ratio. Consequently, when the effective carbon contents are between 0.09 and 0.115 wt%C, most cracks occur. In addition, the longitudinal crack ratio gradually increases and then rapidly decreases thereafter, when the carbon contents are between 0.09 and 0.115 wt%C. When the effective carbon content is 0.106 wt%C, crack generation ratio is maximum.

To understand the behaviors of the longitudinal crack ratio and crack mechanisms, the former according to effective carbon contents is shown with the transition line in Fig. 16. The longitudinal crack ratio increases until 0.106 wt%C at which the maximum crack ratio is generated, and then decrease rapidly, as shown at Fig. 16a. That means the carbon contents of the maximum crack ratio are in the range of 0.104–0108 wt%C. In the previous Sect. 3.3, it is suggested that there are two mechanisms of crack generation, massive transformation

The influence of each alloy element on the change of peritectic points (a and b as shown in Fig. 14) was suggested at the results of Xu et al. [27] They suggested that Al, P, Si, Mn, and S had an individual effect on peritectic points, and the interactions between S and Mn as well as those between Si and Mn cause movements of peritectic points.

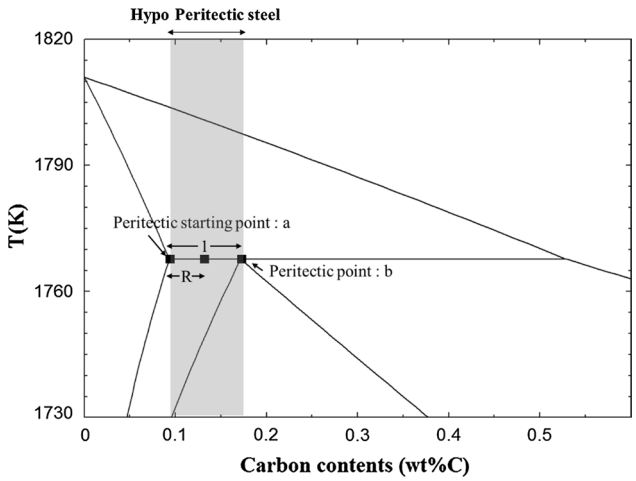

Fig. 14 Values for calculating the relative position in the range of hypo peritectic steel (R)

Table 1 Coefficients of relative position in the region of hypo-peritectic steel.

	a (Al)	b (S)	c (P)	d (Si)	e (Mn)	f (S·Mn)	g (Si·Mn)	h (Constant)	R square
A	3.9997	379.6260	− 22.0576	− 0.5573	2.1889	− 148.275	1.3074	12.3439	0.9584
B	− 0.2476	− 23.7260	1.472	0.0241	0.0197	15.5063	0.1484	− 1.1562	0.9117

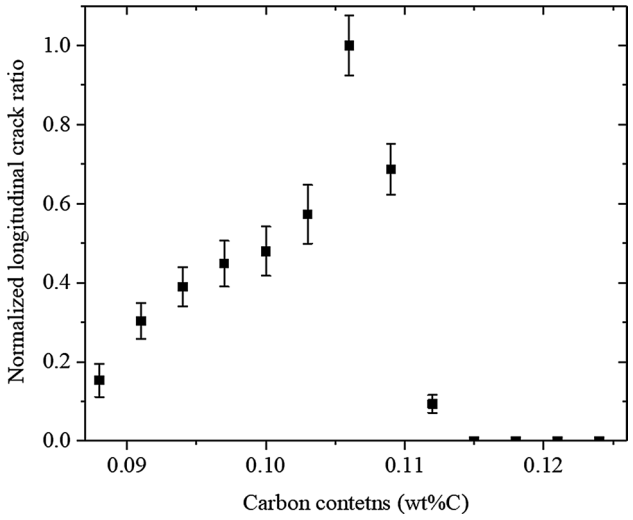

Fig. 15 Relative values of longitudinal crack ratios at every 0.04 interval of the position in hypo-peritectic steel

in solid and peritectic transformation during solidification, and the change of crack mechanisms occurs at a specific region of dT_p and carbon contents on the transition line. Moreover, it is revealed that the possibility of crack generation can be maximized at this condition by maximum strain rates and liquid unfilling possibilities. So, dT_p can be calculated using the transition line with the carbon contents at which the maximum crack ratio is generated, as shown in Fig. 16b. As a result, the dT_p of the results of this field data is 11 K($\pm$1.2 K).

In other words, depending on the carbon composition and dT_p, crack generation mechanisms are selectively employed between the massive transformation in the solid phase and liquid unfilling during solidification. Crack generation behaviors can be predicted according to carbon contents as follows: The possibility of crack generation; (1) increases up to the condition of carbon contents on the transition line; (2) is maximized at the carbon content near the condition on the transition line; and (3) when the carbon contents increase, the possibility of crack generation decreases rapidly.

Many researchers have reported on longitudinal crack ratios according to carbon contents and have also analyzed crack ratio behaviors with their crack mechanism models [1, 23, 24]. In these studies, crack ratio increases, and then decreases upon reaching the maximum value. Furthermore, the carbon contents at which the maximum crack ratio is generated are approximately 0.11 wt%C, 0.129 wt%C, and 0.132 wt%C, respectively. The crack ratio behavior is similar to the results of our field results, as shown in Fig. 15. However, the carbon contents at maximum crack ratio differ from experimental results. This difference can be explained by the difference of dT_p under various experimental conditions. Maximum crack ratio can be generated near the transition line, and the carbon contents with maximum crack ratio increases with dT_p, as shown in Fig. 11. As a result of calculating the normalized dT_p for each experimental condition [1, 23, 24], the values of dT_p are about 14, 24, 29K, respectively. The present study showed that dT_p is a very important parameter for predicting the crack ratio of continuous casting processes of hypo-peritectic steels. Unfortunately, dT_p determination under specific conditions might be very difficult because dT_p could be affected by cooling rates, steel grades, and the conditions of continuous casting machine. However, it is suggested that the dT_p value can be estimated from the carbon contents with maximum crack ratio of each experimental data by the analysis of the present study and the field results employed herein. Thus, it is possible to suggest conditions that can reduce the risk of crack generation through alloy design and the adjustment of operating conditions.

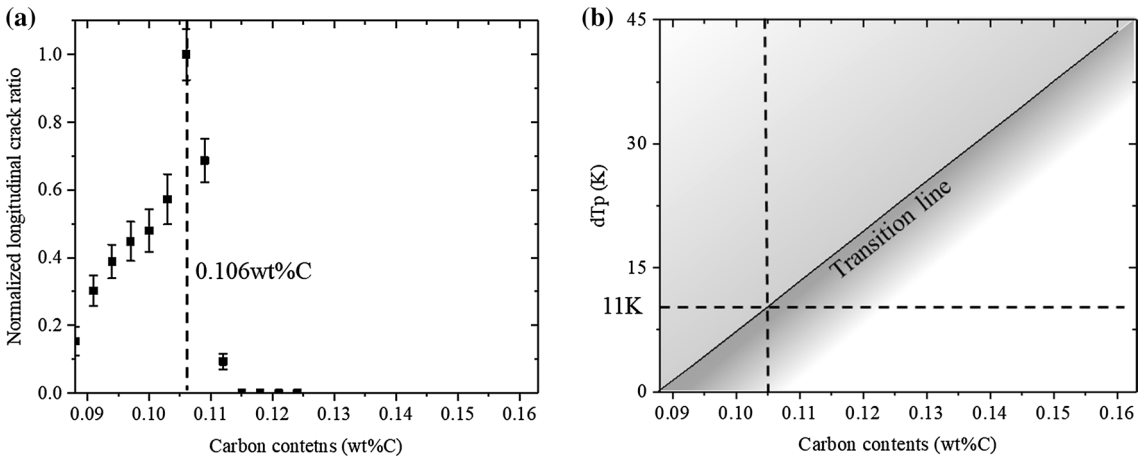

Fig. 16 Mechanisms of crack generation change when carbon content is 0.106 wt%C and dT_p = 11 K

4 Conclusion

It is necessary to understand the phase change behavior of hypo-peritectic steel to analyze crack generation behaviors in continuous casting processes. Stress in the solidified shell and large volume contraction with small liquid fractions were suggested for predicting crack possibilities by many researchers. In this study, We developed a new model that could predict the possibility of crack generation during cooling. These models are based on volume contraction rates with liquid, strain rates in solid, and liquid unfilling possibilities.

From the results of strain rates, volume contraction rates, and liquid unfilling possibilities, it can be suggested that the massive transformation from the δ phase to the γ phase or peritectic transformation during solidification are the main mechanisms for crack generation. The large strain rates in solids are generated when massive transformation from the δ phase to the γ phase occurs. The volume contraction rates become large when peritectic transformation starts with the liquid. In addition, liquid unfilling possibilities are calculated to analyze the penetrating ability of the liquid into the dendrite arm spacing during cooling. Liquid unfilling possibilities have small values at the low carbon regions of hypo-peritectic steels, and are maximized by peritectic transformation during solidification. Furthermore, liquid unfilling possibilities decrease rapidly with the increase of the liquid fraction where peritectic transformation starts.

From the results of maximum strain rates and liquid unfilling possibilities, it was revealed that there are relationships between carbon contents and dT_p for crack generation mechanisms. On the left-hand side of the transition line, massive transformation in solid is main crack mechanism, while on the right-hand side of the transition line, peritectic transformation during solidification is main crack mechanism. In addition, it was suggested that the possibility of crack generation could be maximized near the condition represented on the transition line.

These results of maximum strain rates in solid and liquid unfilling possibilities were compared with longitudinal crack ratio data from the continuous casting process. The relative position in the range of hypo-peritectic steel and effective carbon content are suggested for applying the crack ratio data of steels with various alloy elements to the results of the crack mechanism model of carbon steel. As a result of the crack ratio data using effective carbon content, the crack ratio gradually increases from low carbon content in the region of hypo-peritectic steel, rapidly increases up to the maximum crack ratio near a specific carbon content on the transition line, and then rapidly decreases. Thus, this crack generation tendency can be analyzed using maximum strain rates in solid and liquid unfilling possibilities, and it is revealed that there are specific dT_p and carbon content at which the maximum crack ratio can be generated. Furthermore, various carbon contents with maximum crack ratio according to experiments can be explained by the dT_p difference.

Reference

1. J. Xu, S. He, X. Jiang, T. Wu, Q. Wang, ISIJ Int. **53**, 1812 (2013)
2. M. Suzuki, Y. Yamaoka, Mater. Trans. **44**, 836 (2003)
3. S. Koric, B.G. Thomas, J. Mater. Process. Technol. **197**, 408 (2008)
4. C. Li, B.G. Thomas, Metall. Mater. Trans. B **35**, 1151 (2004)
5. S. Koric, B.G. Thomas, J. Mater. Process. Technol. **197**, 408 (2008)
6. M.L. Zappulla, L.C. Hibbeler, B.G. Thomas, Metall. Mater. Trans. A **48**, 3777 (2017)
7. K. Kim, T.-J. Yeo, K.H. Oh, D.N. Lee, ISIJ Int. **36**, 284 (1996)
8. J. Borland, Br. Weld. J. **7**, 508 (1960)
9. T. Clyne, M. Wolf, W. Kurz, Metall. Trans. B **13**, 259 (1982)
10. E.A. López, M.H. Trejo, J.J.R. Mondragón, M. d. J. C. Román, H.S. Tovar, ISIJ Int. **49**, 851 (2009)
11. D. Phelan, M. Reid, R. Dippenaar, Metall. Mater. Trans. A **37**, 985 (2006)
12. H. Mizukami, A. Yamanaka, T. Watanabe, ISIJ Int. **42**, 964 (2002)
13. H. Shibata, Y. Arai, M. Suzuki, T. Emi, Metall. Mater. Trans. B **31**, 981 (2000)
14. S.-C. Moon, R. Dippenaar, S.-H. Lee, *IOP Conference Series: Materials Science and Engineering*, The 3rd International Conference on Advances in Solidification Processes, Aachen, The Netherlands, June 7–10, 2011. Vol. 27 (IOP Publishing, Bristol, 2012), p. 012061
15. S. Griesser, C. Bernhard, R. Dippenaar, Acta Mater. **81**, 111 (2014)
16. J.J.R. Mondragón, M. H. Trejo, M. d. J. C. Román. ISIJ Int. **48**, 454 (2008)
17. C. Cicutti, R. Boeri, Steel Res. Int. **77**, 194 (2006)
18. J. Jo, K. Yi, Met. Mater. Int. (2020). https://doi.org/10.1007/s12540-019-00593-9
19. J. Lemaitre, J.-L. Chaboche, *Mechanics of Solid Materials*. Cambridge University Press, Cambridge (1994)
20. Nippon Kikai Gakkai (ed.), *JSME Mechanical Engineers' Handbook (Kikai Kogaku Binran)* (Japan Society of Mechanical Engineers, Tokyo, 1987), p. A4–12
21. Y.M. Won, H.N. Han, T. Yeo, K.H. Oh, ISIJ Int. **40**, 129 (2000)
22. J. Konishi, M. Militzer, I. Samarasekera, J. Brimacombe, Metall. Mater. Trans. B **33**, 413 (2002)
23. Y. Miyashita, M. Suzuki, K. Taguchi, S. Uchida, H. Sato, M. Yamamoto, Nippon Kokan Tech. Rep. **93**, 178 (1982)
24. T. Ueda, H. Hirahara, A. Kuwabara, T. Watanabe, K. Matsui, Tetsu-to-Hagane **67**, 1236 (1981)
25. S.-C. Moon, R. Dippenaar, S.-Y. Kim, *AISTech - Iron and Steel Technology Conference Proceedings*, ASITech 2015: The Iron & Steel Technology Conference and Exposition, Ohio, USA, May 4-7, 2015. Vol. 12 (Iron and Steel Society, Warrendale, 2015), p. 111
26. Y. Ueshima, S. Mizoguchi, T. Matsumiya, H. Kajioka, Metall. Trans. B **17**, 845 (1986)
27. J. Xu, S. He, T. Wu, X. Long, Q. Wang, ISIJ Int. **52**, 1856 (2012)